EFFECTS OF VARIABILITY ASSOCIATED WITH THE ANTARCTIC CIRCUMPOLAR CURRENT ON SOUND PROPAGATION IN THE OCEAN

Catherine de Groot-Hedlin[1], Donna K. Blackman[1], and C. Scott Jenkins[2]

Scripps Institution of Oceanography, University of California at San Diego[1],
Naval Surface Warfare Center, Indian Head Division[2]

Sponsored by Army Space and Missile Defense Command

Contract No. W9113M-05-1-0019

ABSTRACT

A series of small depth charges was detonated along a transect from New Zealand to Antarctica over a period of three days in late December of 2006. Signals were recorded by hydrophones deployed near the source, and at a sparse network of permanent hydrophone stations operated by the International Monitoring System (IMS), at distances up to 9,600 km. Our purpose was to determine how well signal characteristics could be predicted by the World Ocean Atlas 2005 (WOA05) climatological database for sources within the Antarctic Circumpolar Current (ACC). Where recorded signal to noise ratios are high, travel times and signal dispersion are predicted to within two seconds under the assumption that propagation is adiabatic and follows a geodesic path. The deflection of the transmission path by abrupt spatial variations in sound speed at the northern ACC boundary is predicted to decrease travel times to the IMS stations by several seconds, depending on the path. The accuracy of source locations estimates based only on travel times depends on the monthly or seasonal database used to predict velocities and on whether we account for path deflection. The configuration of the IMS hydrophones limits source location accuracy within the ACC. Comparison of signal spectra for recordings near the source and at distance show that transmission loss is nearly uniform as a function of frequency.

Report Documentation Page

Form Approved
OMB No. 0704-0188

1. REPORT DATE	2. REPORT TYPE	3. DATES COVERED
SEP 2008		**00-00-2008 to 00-00-2008**

4. TITLE AND SUBTITLE	5a. CONTRACT NUMBER
Effects of Variability Associated with the Antarctic Circumpolar Current on Sound Propagation in the Ocean	5b. GRANT NUMBER
	5c. PROGRAM ELEMENT NUMBER
6. AUTHOR(S)	5d. PROJECT NUMBER
	5e. TASK NUMBER
	5f. WORK UNIT NUMBER
7. PERFORMING ORGANIZATION NAME(S) AND ADDRESS(ES) **Naval Surface Warfare Center,Indian Head Division,3767 Strauss Ave Ste 113,Indian Head,MD,20640**	8. PERFORMING ORGANIZATION REPORT NUMBER
9. SPONSORING/MONITORING AGENCY NAME(S) AND ADDRESS(ES)	10. SPONSOR/MONITOR'S ACRONYM(S)
	11. SPONSOR/MONITOR'S REPORT NUMBER(S)

12. DISTRIBUTION/AVAILABILITY STATEMENT
Approved for public release; distribution unlimited

13. SUPPLEMENTARY NOTES
Proceedings of the 30th Monitoring Research Review: Ground-Based Nuclear Explosion Monitoring Technologies, 23-25 Sep 2008, Portsmouth, VA sponsored by the National Nuclear Security Administration (NNSA) and the Air Force Research Laboratory (AFRL)

14. ABSTRACT
see report

15. SUBJECT TERMS

16. SECURITY CLASSIFICATION OF:			17. LIMITATION OF ABSTRACT	18. NUMBER OF PAGES	19a. NAME OF RESPONSIBLE PERSON
a. REPORT	b. ABSTRACT	c. THIS PAGE			
unclassified	**unclassified**	**unclassified**	**Same as Report (SAR)**	**10**	

OBJECTIVES

Our objectives were to conduct a series of calibration shots within and to the south of the ACC that would generate acoustic signals at frequencies f > 30 Hz and to analyze the signals recorded at hydrophone stations operated by the IMS. The overall goal was to compare observed source-receiver travel times to the IMS hydrophone stations to those predicted by numerical models for paths crossing the Antarctic convergence zone and to use these results to determine the accuracy to which sources may be located within the ACC. A second goal was to compare observed vs. modeled transmission losses. The results of the second goal were reported last year; it was found that transmission loss is nearly uniform as a function of frequency for the shots examined in this study (de Groot-Hedlin et al., 2007; de Groot-Hedlin et al., 2008).

Acoustic propagation for sources within the ACC is complicated by the sharp temperature gradient at the northern boundary. The ACC boundary separates cold waters that flow eastward around Antarctica from warmer subtropical waters to the north. The abrupt spatial variation in temperature and salinity results in strong gradients in the speed of acoustic waves through the ocean, which in turn deflects the path of propagating acoustic waves near the northern boundary of the ACC (Heaney et al., 1999). Furthermore, south of the ACC boundary, the low-velocity oceanic "sound channel" axis, that is typically 100's to 1,000-m-deep shoals and the overlying higher velocity layer thins to nothing over a short distance, resulting in sea surface-limited propagation. Therefore, the detailed structure of the ACC boundary is strongly affected by seasonal temperature variations that extend to depths of over 1 km. Dushaw et al., (1999) showed that this type of seasonal variability produces considerable seasonal differences in acoustic travel times for paths through the North Pacific.

We conducted an experiment in December, 2006, to determine how well acoustic wave travel times and signal dispersion are predicted by models derived from the World Ocean Atlas 2005 (WOA05) global ocean climatology database. A series of small explosive sources provided acoustic signals along a single transect between New Zealand and Antarctica. The hydrophone stations are operated by the IMS that recorded the signals, allowing a comparison between observed and predicted signals. The recordings of the detonations provide ground-truth data, allowing us to compare the effect of lateral refraction on travel times and arrival estimates with predictions, and to estimate the effect of surface-limited propagation on source spectra. Thus, we may evaluate the accuracy of location estimates both for sources within the ACC and signals with propagation paths crossing the ACC.

The results reported here are initial steps in characterizing the effects of high temperature and salinity gradients near the ACC on acoustic propagation. Since our experiment was carried out over a time span of just a few days, we are not able to compare predictions with observations of a seasonal cycle, much less several seasons. However, these initial observations allow the scale of the differences between predictions and the data to be assessed, and we find that they are not negligible. In addition to specific comparisons based on the initial dataset, we assess the range in variability in signal characteristics that are predicted throughout the year, based on the long-term monthly/seasonal averages. Again, the predictions indicate that seasonal acoustic variability (travel-time, signal duration, coda shape) should be significant enough to be detectable and to affect determinations of source location.

RESEARCH ACCOMPLISHED

Signals Underwater Sound (SUS) Depth Charges

Our experiment was conducted during the first part of a research cruise whose main effort was a separate study to be conducted in the northwest Ross Sea. The ship departed Lyttleton, New Zealand, and eventually arrived at McMurdo station in Antarctica. Over a period of three days during the first week of the cruise, explosive charges were detonated at six deployment sites. Water depths at the sites ranged from about 800 m to over 4 km. We used 1.8 kg SUS charges (M 59 mod1a) due to their ease of deployment in rough seas, which are common along the Southern Ocean crossing, and because SUS charges generate a high-energy signal over a broad frequency range. The sources were pre-set to detonate at depths of 305 m, 460 m, or 610 m.

Explosive charges were hand-dropped at each deployment site, starting from the shallowest detonation settings and working to the deepest. The ship speed slowed to approximately 1–2 knots during each set of deployments, which lasted from 20–30 minutes. A hydrophone was hand-deployed from the ship's deck to obtain a near-source (hundreds of meters) recording of the signal. Charge depths were confirmed using a semi-empirical equation relating the depth of the charge to the bubble pulse period for an underwater explosion far from either the free surface or the

sea floor. Several larger shots, using a combination of two or three 1.8-kg charges were tested at the last two deployment sites in an attempt to improve detections at the more distant stations and to vary the spectral content of the signal. Shot deployment sites were listed in Table 1 of de Groot-Hedlin et al., (2007); the geodesic paths from each site to the IMS hydrophones are shown in Figure 1.

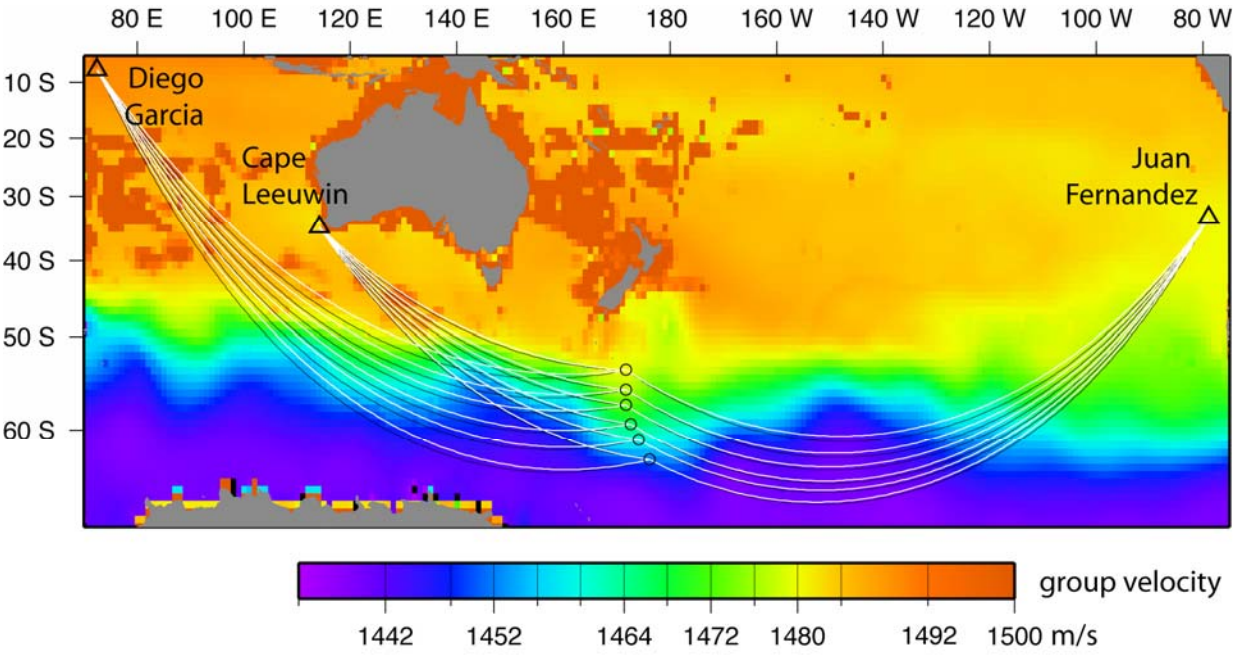

Figure 1. Map showing shot locations (circles) and IMS hydrophone station locations (triangles), superimposed on a map of group velocities derived using average fall sound speed profiles for mode 1 at a frequency of 50 Hz. Geodesic paths (black) and laterally deflected sound paths (white) corresponding to minimum travel-time paths are shown from each shot to each IMS hydrophone.

Near-Source Hydrophone

The near-source hydrophone deployed from the ship recorded the pressure signal of the explosive shots at a rate of 1,000 samples/s. A GPS time sync from the ship's navigation system was fed into the data logger to provide accurate timing. The depth of the near-source hydrophone depth was consistently shallow—from 4 to 6 m—due to the ship's forward motion and the relatively small 4-kg weight used to sink the hydrophone. As a result, signals measured at the hydrophone have two main propagation paths: the direct path and an amplitude-reversed echo from the water surface. Seafloor reverberations were recorded only at the first deployment site where water depths were shallowest *(about 810 m*); they were not evident in unfiltered data at the other stations, where seafloor depths ranged from 3,800–5,400 m. The surface reflection has a small time delay *dt* with respect to the direct path due to its slightly greater path length. The patterns of constructive and destructive interference caused by surface reflection had to be removed from the near-source spectra in order to compare signal spectra with those measured at the IMS hydrophone stations. The method for removing the effects of the surface echo from the source spectra is outlined in detail in de Groot-Hedlin et al., (2008). Here, we simply note that deconvolution adds a measure of uncertainly to the source spectrum estimates. We estimate an uncertainty of about 3 dB in the source spectrum estimates.

Detections and Transmission Losses

The shot locations provided several unblocked paths to arrays at three IMS stations: H01, located near Cape Leeuwin off the southwest coast of Australia, H08 near Diego Garcia island in the Indian Ocean, and H03 near Juan Fernandez island in the Pacific Ocean west of Chile. Background noise levels at each of the hydrophone stations did not vary significantly over the duration of the study. As illustrated in Figure 1, the Cape Leeuwin station (H01) was situated nearest the test shots, at a distance of approximately 5,000 km, as compared to approximately 8,000 km to H03N near Juan Fernandez and 9,600 km to H08S near Diego Garcia. The transmission paths are not entirely free of topographic blockages; for most paths, there is a ridge or plateau that projects at least partway into the sound channel and strips off the highest-order modes. All shots were recorded at H01 with the exception of the second set

of shots at site A2. Apparently, acoustic energy was scattered by shallow features along the Macquarie Ridge that are not resolved in the current global bathymetric database.

Only the first set of shots at site A1, near 53.8°N, 171.7°E, was clearly discernible at station H03N north of Juan Fernandez Island. Recordings of the shots at the remaining sites are difficult to distinguish from background noise levels. The receiver to source back-azimuth varies slightly as the shot locations progressed from north to south. This is sufficient to put H03N into an acoustic shadow zone created by Juan Fernandez Island for the shots at sites A2 through A6. Unfortunately, the southern triplet of the Juan Fernandez station was not in operation during our experiment. Signals were observed at station H08S, south of Diego Garcia for sites A2 through A6. The lack of arrivals for shots at site A1 is likely due to the longer transit over the shallow water depths of the Campbell Plateau south of New Zealand. The Chagos Archipelago blocked acoustic transmission to the northern triplet at Diego Garcia. Another IMS hydrophone station near Crozet Island was also not operational during the experiment, but it was almost certainly blocked by the Kerguelen Plateau anyway. Transmission losses were found to be fairly uniform over the 30-100 Hz band for propagation paths used in this experiment (de Groot-Hedlin et al., 2007).

Comparison of Observed and Predicted Travel Times

In this section we examine the effects of the temporal and spatial variability of sound speeds along propagation paths crossing the northern boundary of the ACC on predicted arrival times, and compare these with observations. Hydroacoustic phases are often represented as a suite of acoustic modes, which are derived from the Helmholtz equation that governs acoustic propagation at a given frequency. Each mode has a local velocity defined by the sound speed profile. In deep water with a well-defined sound speed minimum, low-order modes are associated with rays that propagate at shallow angles near the sound channel axis, and higher-order modes are linked to steeper rays that sample a greater vertical extent of the ocean. A common simplifying assumption is that propagation is adiabatic, that is, each mode propagates independently of the others, with a velocity and amplitude that varies slowly within the nearly range-independent waveguide. This assumption holds in a range-independent medium where the lower order modes are typically the highest amplitude arrivals at the end of the acoustic coda. However, in a more realistic environment, significant coupling of energy between modes occurs due to internal waves (Wage et al., 2005) or propagation through a polar front (Shang and Wang, 1999), resulting in the temporal spreading of acoustic arrivals.

Ocean sound speed profiles are derived from the World Ocean Atlas 2005 database, which gives salinity (Antonov et al., 2006) and temperature (Locarnini et al., 2006) values as a function of depth on a 1° grid. Sea floor depths are derived from ETOPO1, a global 1-minute gridded database of bathymetry and topography; the bathymetry is derived from satellite altimetry and ship depth soundings as described in Smith and Sandwell (1997). Sediment thicknesses are from Mooney et al., (1998). Sediment velocities are assigned a value of 1,550m/s at the seafloor, increasing by 1m/s per meter depth, in line with sea floor sediment velocity estimates from (Hamilton, 1980). The basement structure was assigned a velocity of 2,600 m/s.

Sound speeds along a path from site A3 to H01 are shown in Figure 2a for average October–December season profiles. Path variations in ocean temperatures, and hence sound speeds, are greatest above the sound channel axis. Ocean sound speed profiles along this path can be classified into three types. A polar channel exists to a range of approximately 2,500 km. Within this section, sound speeds reach a minimum near the surface; therefore, acoustic energy is surface limited—trapped between the surface and sound-speed gradients at depth. Propagation paths from the calibration shots to H01 cross the polar front at the northern boundary of the ACC near 50°S. A double channel extends from a range of about 2,500 km to 4,000 km; acoustic energy may become trapped within the surface duct within this region. The final segment consists of a single duct with a well-defined Sound Fixing and Ranging (SOFAR) channel.

Group velocities are shown in Figure 2b for several modes along this path for a 50-Hz source—where signal-to-noise ratio (SNR) is high. Because low-order modes propagate at depths near the sound speed minimum, the contrast in velocity is greatest across the ACC. A large contrast in sound speeds across the ACC boundary is linked with greater horizontal refraction there. Because higher order modes typically sample a greater vertical extent, they undergo greater interaction with the seafloor, and thus greater attenuation. Group velocities for high order, bottom-interacting modes are more poorly constrained than for low-order modes because sea-floor velocities are known only approximately.

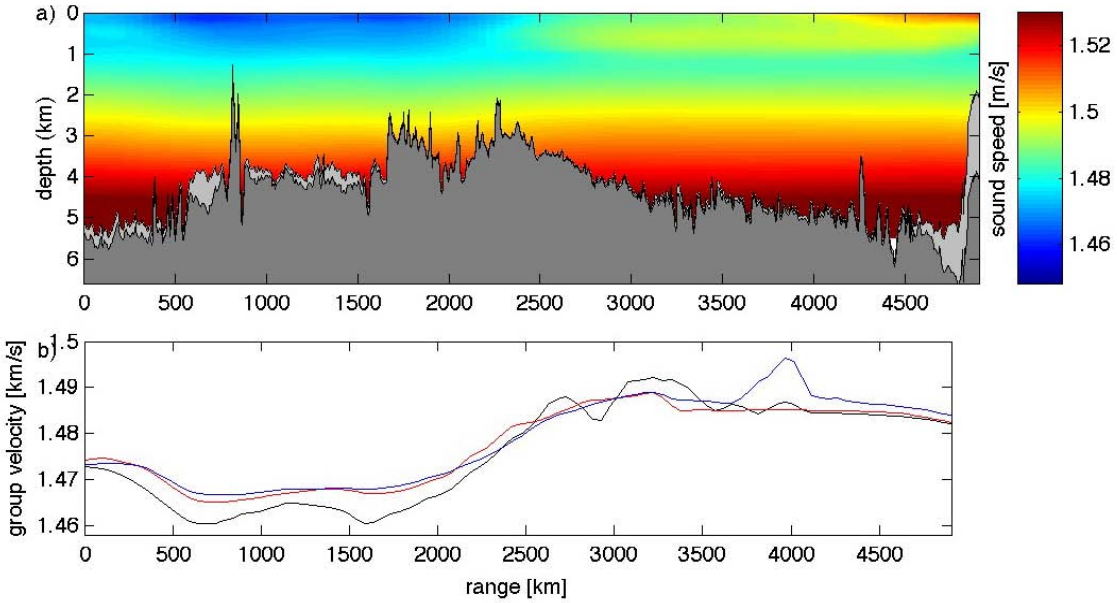

Figure 2. a) Average fall (October-December) sound speed profile along the geodesic path from the first shot at site A3 to the hydrophone triplet at H01. Sound speeds are derived from the WOA05 database; bathymetry is from Smith and Sandwell (1997). Sediments, indicated in light gray, are underlain by a basement structure, shown in dark gray. b) Group velocities along the path for a 50-Hz source are shown for mode 1 (black), mode 4 (red), and mode 8 (blue).

Figure 3 illustrates variations in the first 10 modes for a 50-Hz source at points along the propagation path near the source, within the double sound channel, and in the SOFAR channel. A comparison of mode shapes within the polar channel with those along the remainder of the path indicates that propagation of these acoustic modes is confined much closer to the surface within the ACC and are thus less subject to mode-stripping by bathymetric features. Modal degeneration occurs where adjacent modes have identical wave numbers. This occurs where modes become trapped in the upper duct of a double-channel feature and result in travel-time miscalculation (Shang and Wang, 1999), if the modes are assumed to be adiabatic. As shown in Figure 2b, the double-channel feature is associated with a significant variation in group velocity, particularly for higher-order modes. Seafloor depths near H01 are on the order of 1.6 km; thus, higher order modes interact with the seafloor at a frequency of 50 Hz for propagation near the IMS receiver.

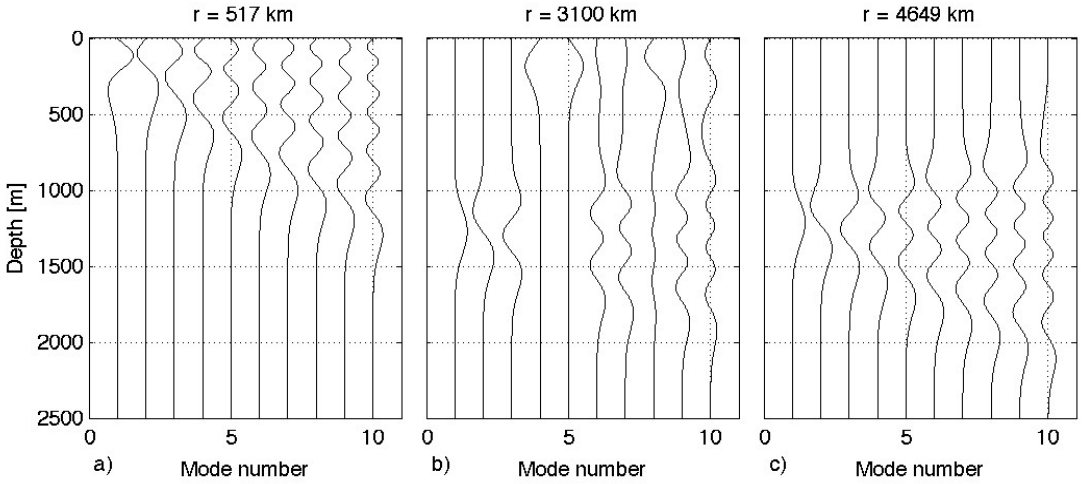

Figure 3. Mode shapes at 50 Hz at several distances along the receiver path for the environmental model shown in Figure 2a. Mode shapes for a) the polar channel near the source, b) within the double sound channel, and c) within the SOFAR channel. All modes were computed for deep water profiles, with seafloor depths greater than 4,000 km.

Travel times to a distant receiver are often computed under the assumptions that there is no significant lateral deflection of the travel path (e.g., Chapp et al., 2005), and that propagation is adiabatic, as discussed earlier. In this case, travel times may be computed by integrating the group velocities for a given mode along a geodesic path. The variation in the travel times for each mode gives an estimate of the duration of the arrival. The amplitude at the receiver at a given frequency is given by the formula in Jensen et al., (1994). The attenuation for each mode is given by the fraction of that mode's intensity within the attenuation seafloor, as in Heaney et al., (1991). Figure 4a shows predicted arrivals for the first 25 normal modes for adiabatic propagation from a 50-Hz source at a 300-m depth at site A3 to the first hydrophone within the H01 triplet. The environmental model and modal group velocities were illustrated in Figure 2a. Amplitudes are scaled with respect to the largest modal amplitude, mode 1 in this case. If propagation was adiabatic, the figure indicates that the recorded wavetrain would consist of a series of discrete pulses with mode 1 arriving last and having the largest amplitude.

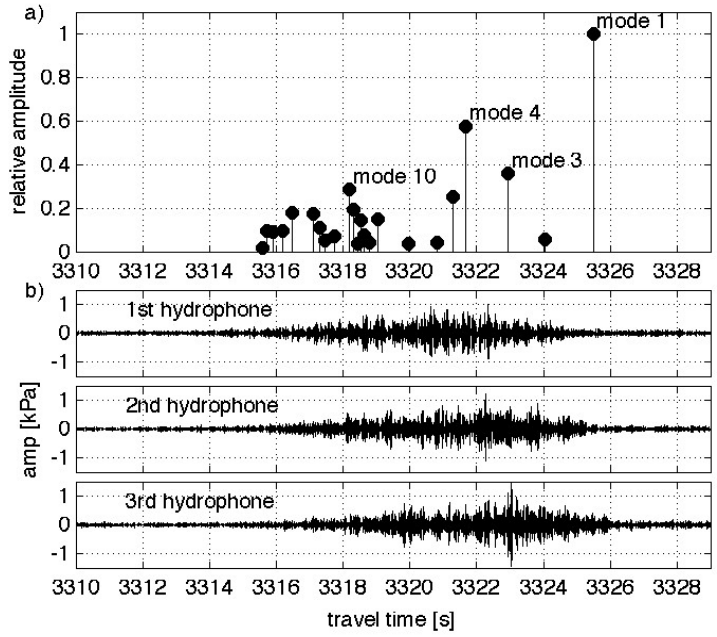

Figure 4. **a) Synthetic wavetrain (relative magnitudes are true; mode 1 is set to have an amplitude of 1 here) for adiabatic propagation from a 50-Hz source at a 300-m depth for the October-December average environmental model shown in Figure 2a, computed for the first hydrophone within the triplet at H01. The four highest amplitude modes are labeled. Mode amplitudes are normalized with respect to mode 1. b) Pressure (in kPa) recorded at each hydrophone within the array at H01 for a charge detonated at a300-m depth at site A3.**

For comparison, Figure 4b shows the wavetrains recorded on each hydrophone at H01 for the first charge at site A3, bandpassed from 45–55 Hz. The coda have a duration of less than 10 s, have a maximum amplitude near the center of the wavetrain, and end nearly a second early compared with the predicted maximum amplitude arrival associated with the first mode. The source had a duration of approximately 0.1 s as observed on the near-source hydrophone; therefore the lack of impulsive arrivals cannot be attributed to the source duration. Rather, the phase duration is attributable to mode dispersion; mode velocity increases with the increasing mode number, with an average group velocity of 1,480.2 m/s for the 25th mode, and 1,475.9 m/s for the first mode. The phase shape does not correspond to an energetic late arrival or discrete arrivals corresponding to individual modes as predicted by adiabatic mode theory, implying that significant mode coupling takes place along the propagation path. This suggests that picking acoustic arrival times based on the peak amplitude mode, as in Hanson et al., (2001), would lead to errors in source location as this choice relies on the adiabatic mode approximation. Although Figure 4 illustrates that the shape of the arrival is not correctly predicted by the adiabatic mode interpretation, the arrival onset and total duration of the arrival are predicted to an accuracy of approximately 2 s.

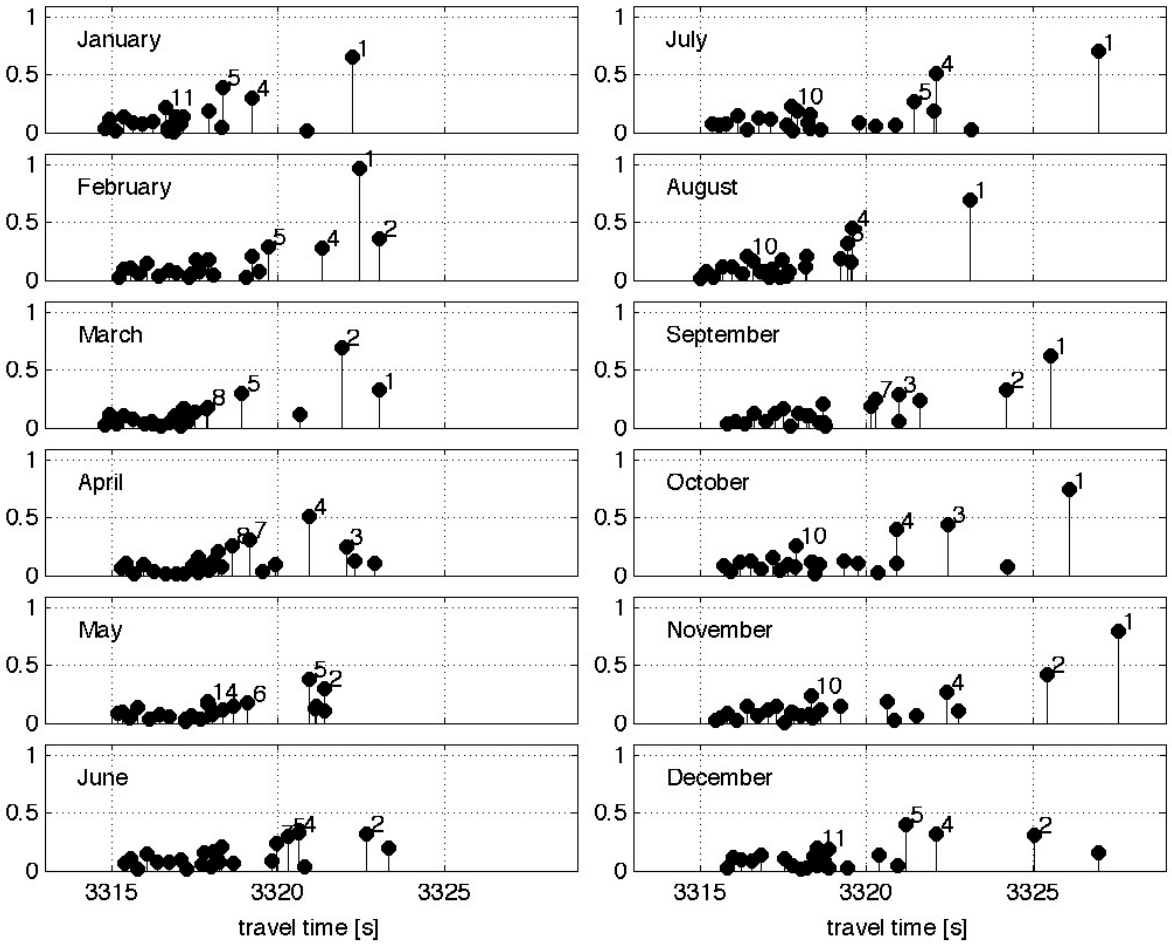

Figure 5. a) Mode arrival times and amplitudes for adiabatic propagation from a 50-Hz source at a 300-m depth for site A3 to station H01, for the first 25 modes. The four highest amplitude modes are labeled for each month. Mode amplitudes are normalized with respect to the largest arrival over all months—mode 1 in February.

Similar adiabatic mode computations were performed for the path from the first charge at site A3 to the first hydrophone at station H01 for each month of the year (Figure 5). Monthly temperature and salinity data from the WOA05 database are available to depths of 1,500 m and were extended to a depth of 5,500 m by merging them with the annual average data. A cosine taper was used to ensure smooth transitions between monthly and annual data. The coda onset times are predicted to vary little throughout the year, but the shape of the coda and degree of dispersion are predicted to change significantly. Early arrivals tend to be emergent, making it difficult to pick precise arrival onset times, and may undergo sea floor interaction. Increasing interaction with the sea floor leads both to enhanced attenuation and higher propagation speeds; thus, group velocities associated with the arrival onset may be poorly constrained. By contrast, the mode-1 travel time is predicted to vary significantly throughout the year, suggesting that small changes in the environmental model can lead to significant variations in predicted arrival times for the lowest-order modes, and hence the total phase duration. For example, the mode-1 arrival time and total coda duration is predicted to change by 5 to 6 s from December to January, indicating that monthly variations in sound-speed profiles lead to relatively large differences in computed travel times for this particular path. This implies that near-surface temperatures, which are sensitive to fluctuations in the weather, may affect computed acoustic travel times and durations in polar regions. Thus, the WOA05 climatology database, which is based on long-term averages, may be inadequate to compute arrival times for low-order modes to better than several seconds for sources within the ACC. More detailed ocean models are needed if greater accuracy is required.

These synthetic "wavetrains" were computed and compared to arrivals for 14 shots at sites A3–A6. In each case, the results confirmed that adiabatic mode theory correctly predicts several features of the arrivals. First, given equal charge sizes at a given site location, the shallowest ones—at 300 m depth—yield arrivals with the greatest signal strength at Cape Leeuwin. Secondly, the signal duration does not depend on either the charge depth or size. Thirdly, the duration increases for sources further to the south, indicating greater signal dispersion for longer propagation paths within the ACC. However, comparison of recorded waveforms with the synthetic wavetrain consisting of the first 25 modes confirms that the shape of the coda is not well predicted by adiabatic mode theory, again suggesting coupling between the modes along the propagation path.

The average group velocities along the propagation path vary from 1,475.9 m/s for mode 1 to 1,480.2 m/s for mode 25 at site A3, for a duration of 10 s at this site, decreasing to 1,467.4 m/s for mode 1 and 1476.4 m/s for mode 25 at site A6, for a total duration of 22 s. Thus, average along-path velocities depend on the source position; therefore, a single average acoustic velocity cannot be used to estimate travel time for sources within the ACC, as is done for sources further to the north (Blackman et al., 2004).

Source Location Estimates

In the previous section, travel times were computed for propagation along a geodesic path, which is the minimum-distance path between any two points. By Fermat's principle, the acoustic propagation path between two points is the least-time path, not the minimum-distance path. Thus, there can be significant deflection from a geodesic at polar latitudes due to large horizontal gradients in the modal velocities at the ACC boundary (Heaney et al., 1991). The deflection affects both travel times and back azimuths measured at the receiver, and thus impacts source location estimates. The degree of deflection at a given mode and frequency may be estimated using group velocities derived from the WOA05 database, which yields a smoothed representation of the actual spatial variations in velocity. A minimum-time raypath is then computed between any two given points using a perturbation method.

Figure 6 shows both the geodesic path and the deflected paths from each shot site to each IMS hydrophone station, superimposed on a map of the group velocities derived from October–December sound speed profiles for mode 1 at a frequency of 50 Hz. As indicated, there is a significant increase in group velocities from south to north across the ACC, thus ray-bending is significant. Ray-bending decreases the travel time to the Diego Garcia stations by 2.8 to 5.6 s, by 1.1 to 3.9 s to Juan Fernandez, and by 0.3 to 1.5 s to Cape Leeuwin, as compared to propagation along geodesic paths from each source to the receivers. The bending of the sound path deflects the back azimuths by 5.6^{o} from A1 to 8.7^{o} from A6 at Diego Garcia, by 5.7^{o} from A1 to 2.3^{o} from A6 at Juan Fernandez, and 1.1^{o} from A1 to 2.5^{o} from A6 at Cape Leeuwin. The contrast in group velocities across the ACC decreases somewhat at higher modes; thus, ray-bending is most significant for the lowest-order modes.

Back azimuths from multi-instrument stations can be computed to high precision by cross-correlating signals over a narrow frequency band and finding the best plane wave solution to the relative delay times. However, the degree of correlation decreases as the number of wavelengths between each hydrophone pairs increases. For the IMS stations, hydrophone pairs are each about 2 km apart, and cross-correlations are most effective at frequencies of 15 Hz or less. Low SNR at frequencies less than 20 Hz made this method infeasible for this experiment. Instead, azimuths measured from source to receiver were derived using cross-correlations of the envelopes of signal code between pairs of hydrophones within each station's triad. We estimated the azimuths over a number of frequency bands at each station to quantify the uncertainty in our estimates. Unfortunately, the azimuths derived in this way had an error of at least 7^{o} for each source-station pair, too large to use in deriving source locations.

Source location estimates were therefore derived using travel-time information only for shots that were recorded at two IMS stations; shots at sites A1 were recorded at both H01 and H03N; shots at A3 through A6 were recorded at both H01 and H08S; shots at site A2 were recorded at only one station. Arrival time picks were made at the end of the waveform because the lowest order modes arrive latest and are the most robust, i.e., the ones that undergo the least seafloor interaction. However, the drawback is that total travel times for the lowest-order modes vary seasonally, by up to 6 s as shown in Figure 5.

Source location estimates made using only travel time differences between pairs of observing stations are compared in Figure 6 for the cases where acoustic propagation is assumed to occur along geodesic paths, and where lateral diffraction is taken into account. In each case, the source locations were derived under the assumption that

travel-time differences are accurate to six seconds. Location estimates were derived from mode-1 group velocities for December, January, autumn (October through December) and winter (January through March). As shown, recordings made at Juan Fernandez and Cape Leeuwin yield source estimates that are more poorly constrained in latitude than in longitude, i.e., site A1, while the reverse is true for sources recorded at Cape Leeuwin and Diego Garcia (sites A3 through A6). Source location estimates for A1 have a precision of approximately 0.15° in longitude, or about 10 km, while source location estimates at A3 through A6 have a precision of approximately 0.5° in latitude, or about 55 km. The effects of seasonal variations in the WOA05 profiles make less difference in source location estimates than the effects of ray bending. In any scenario, the source location estimates for site A6 are biased southward with respect to the true location. The error at site A6 lies in differences of 6–10 s between observed and computed travel times to Cape Leeuwin. The error could arise from the misidentification of the end of the waveform due to the low SNR, or travel times could be overestimated if ocean models are inaccurate.

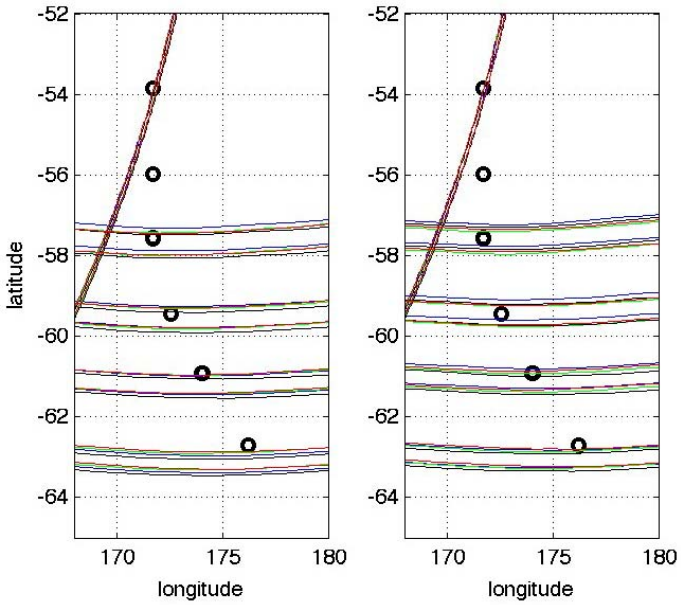

Figure 6. Location estimates derived using travel differences between pairs of stations. Group velocities were derived from WOA05 profiles for December (blue), January (green), October-December (black) and January-March (red). The map at left shows source location estimates corresponding to propagation along geodesic paths, with actual source locations marked by circles. Source locations derived taking ray-bending into account are shown at right.

CONCLUSIONS AND RECOMMENDATIONS

The major findings of this study are the following:

1) Transmission losses are nearly uniform as a function of frequency for paths examined in this experiment. This was shown in de Groot-Hedlin (2007) and de Groot-Hedlin (2008).
2) Signal dispersion increases with the length of the propagation path through the ACC, in agreement with predictions. In this experiment, signal duration increased for shots furthest to the south. For instance, the distance from shot sites A3 through A6 to Cape Leeuwin increased from 4,900 km to 5,200 km, but the signal duration more than doubled from 10 s to 22 s. Since surface propagation varies throughout the year, there is a significant amount of seasonal variability in the signal duration.
3) Travel times computed under the adiabatic assumption were reasonably accurate for the source locations used in this study; at Cape Leeuwin where the SNR was high, there were 2 s between measured and predicted travel times and durations. However, travel times and signal dispersion are predicted to vary throughout year, especially for the lowest-order modes, which undergo surface-limited propagation within the ACC. More detailed ocean models are needed to obtain greater accuracy in travel times and durations.
4) Ray bending is predicted to alter the receiver to source azimuth by as much as 8.7° for travel paths that are highly oblique with respect to the boundary. This prediction could not be confirmed by observation in this study because of large errors in the estimated back azimuths at high frequencies; low SNR in the 5–15 Hz band precluded the use of more accurate waveform correlation methods.

5) Source location estimates made using travel times only are improved by taking ray bending into account but the receiver configuration is a larger source of localization error. Source location estimates are well constrained in longitude if arrivals are detected at Juan Fernandez and either Cape Leeuwin or Diego Garcia, but poorly constrained in latitude. Conversely, source-location estimates for signals detected at Cape Leeuwin and Diego Garcia are very poorly constrained in longitude and to only 55-km accuracy in latitude if travel time picks are accurate to 6 s. An accuracy of about 1 s in travel times measured at Cape Leeuwin and Diego Garcia would be required to estimate source locations to within 10 km in latitude. Alternatively, accurate receiver-to-source azimuths, if available, could be used to improve location accuracy, but the large deflections in the propagation path would have to be accounted for.
6) We were limited to an experiment conducted over three days. Further experiments conducted over the entire seasonal cycle and in other regions of the ACC would aid in characterizing seasonal variability in localization of travel times for sources in this area. Sources that generate broader spectrum signals, especially at the lower end of the frequency band measured at the IMS stations, would allow us to accurately estimate source azimuth using waveform cross-correlation methods, and thus aid in characterizing accuracy of source location estimates.

ACKNOWLEDGEMENTS

Brian Dushaw provided helpful suggestions and provided the WOA05 monthly data and code to read the profiles. We thank Steve Cande and JoAnn Stock for allowing us to piggyback the experiment on their research cruise aboard the Nathanial B. Palmer, during which crew support for our work was excellent.

REFERENCES

Antonov, J. I., R. A. Locarnini, T. P. Boyer, A. V. Mishonov, and H. E. Garcia (2006). *World Ocean Atlas 2005, Volume 2: Salinity.* S. Levitus, Ed. NOAA Atlas NESDIS 62, U.S. Government Printing Office, Washington, D.C., 182 pp.

Blackman, D. K., C. de Groot-Hedlin, P. Harben, A. Sauter, and J.A. Orcutt (2004). Testing low/very low frequency acoustic sources for basin-wide propagation in the Indian Ocean, *J. Acoust. Soc. Am.* 116: 2057–2066.

Chapp, E., D. R. Bohnenstiehl, and M. Tolstoy (2005). Sound-channel observations of ice-generated tremor in the IndianOcean, Geochem. *Geophys. Geosyst.* 6, Q06003, doi:10.1029/2004GC000889.

de Groot-Hedlin, C. D., D. K. Blackman, C. S. Jenkins (2007). Hydroacoustic propagation through the Antarctic Convergence Zone, in *Proceedings of the 29th Monitoring Research Review: Ground-Based Nuclear Explosion Monitoring Technologies,* LA-UR-07-5613, Vol. 2, pp. 697–706.

de Groot-Hedlin, C. D., D. K. Blackman, C. S. Jenkins (2008). Effects of variability associated with the Anatarctic Circumpolar Current on sound speed in the ocean, *Geophys. J. Int.*, submitted.

Dushaw, B. D. (1999). Inversion of multimegameter range acoustic data for ocean temperature, *IEEE J. Oceanic Engineering* 24: 215–223.

Hamilton, E. L. (1980). Geoacoustic modeling of the seafloor, *J. Acoust. Soc. Am*. 68: 1313–1340.

Hanson, J., R. Le Bras, P. Dysart, D. Brumbaugh, A. Gault, and J. Guern (2001). Operational processing of hydrocoustics at the Prototype International Data Center, *Pure Appl. Geophys.* 158: 425–456.

Heaney, K. D., W. A. Kuperman, and B. E. McDonald (1991). Perth-Bermuda sound propagation (1960): Adiabatic mode interpretation, *J. Acoust. Soc. Am.* 90: 2586–2594.

Jensen, F. B., W. A. Kuperman, M. B. Porter, and H. Schmidt (1994). *Computational Ocean Acoustics,* AIP, Woodbury, New York.

Locarnini, R. A., A. V. Mishonov, J. I. Antonov, T. P. Boyer, and H. E. Garcia (2006). *World Ocean Atlas 2005, Volume 1: Temperature.* S. Levitus, Ed. NOAA Atlas NESDIS 61, U.S. Government Printing Office, Washington, D.C., 182 pp.

Mooney, W. D., G. Laske and G. Masters, (1998), CRUST5.1: A global crustal model at 5°x5°. *J. Geophys. Res.* 103: 727–747.

Shang, E.C., and Y.Y. Wang (1999). Subarctic frontal effects on long-range acoustic propagation in the North Pacific Ocean, *J. Acoust. Soc. Am.* 105**:** 1592–1595.

Smith, W. H. F., and D. T. Sandwell (1997). Global seafloor topography from satellite altimetry and ship depth soundings, *Science* 277: 1957–1962, 26 Sept.

Wage, K. E., M. A. Dzieciuch, P. F. Worcester, B. M. Howe, and J. A. Mercer (2005). Mode coherence at megameter ranges in the North Pacific Ocean, *J. Acoust. Soc. Am.* 117: 1565–1581.